Termine, J. D., Eanes, E. D., Ein, D., & Glenner, G. G. (1972) *Biopolymers 11*, 1103–1113.
Towbin, H., Staehelin, T., & Gordon, J. (1979) *Proc. Natl. Acad. Sci. U.S.A. 76*, 4350–4354.
Venyaminov, S. Y., & Kalnin, N. N. (1990) *Biopolymers 30*, 1243–1257.
Westaway, D., Goodman, P. A., Mirenda, C. A., McKinley, M. P., Carlson, G. A., & Prusiner, S. B. (1987) *Cell 51*, 651–662.
Wiley, C. A., Burrola, P. G., Buchmeier, M. J., Wooddell, M. K., Barry, R. A., Prusiner, S. B., & Lampert, P. W. (1987) *Lab. Invest. 57*, 646–655.

Conformational Studies of a Peptide Corresponding to a Region of the C-Terminus of Ribonuclease A: Implications as a Potential Chain-Folding Initiation Site†

John M. Beals,‡ Elisha Haas,§,‖ Sara Krausz,§ and Harold A. Scheraga*,‡

Baker Laboratory of Chemistry, Cornell University, Ithaca, New York 14853-1301, Department of Life Sciences, Bar-Ilan University, Ramat-Gan, Israel, and Chemical Physics Department, Weizmann Institute of Science, Rehovot, Israel

Received December 26, 1990; Revised Manuscript Received April 5, 1991

ABSTRACT: Conformational properties of the OT-16 peptide, the C-terminal 20 amino acids of RNase A, were examined by nonradiative energy transfer. A modified OT-16 peptide was prepared by solid-phase synthesis with the inclusion of diaminobutyric acid (DABA) at the C-terminus. The OT-16-DABA peptide was labeled with a fluorescent 1,5-dimethylaminonaphthalene sulfonyl (dansyl, DNS) acceptor at the N-terminal amine and a fluorescent naphthoxyacetic acid (NAA) donor at the γ-amine of the DABA located at the C-terminus of the peptide by using an orthogonal protection scheme. Energy transfer was monitored in DNS-OT-16-DABA-NAA by using both fluorescence intensity (sensitized emisson) and lifetime (donor quenching) experiments. The lifetime data indicate that the peptide system is a dynamic, flexible one. A detailed analysis, based on a dynamic model that includes a skewed Gaussian function to model the equilibrium distribution of interprobe distances and a mutual diffusion coefficient between the two probes to model conformational dynamics in the peptide [Beechem & Haas (1989) *Biophys. J. 55*, 1225.], identified the existence of a partially ordered structure (relatively narrow distribution of interprobe distances) at temperatures $\geq$20 °C in the absence of denaturant. The width and the position of the average of the distributions decrease with increasing temperature, in this range; this suggests that the structure is stabilized by hydrophobic interactions. In addition, the peptide undergoes cold denaturation at around 1.5 °C as indicated by broadening of the distance distribution. The addition of 6 M guanidine hydrochloride (Gdn-HCl) also broadens the distance distribution significantly, presumably by eliminating the hydrophobic interactions and unfolding the peptide. The results of the analysis of the distance distribution demonstrate that (1) nonradiative energy transfer can be used to study the conformational dynamics of peptides on the nanosecond time scale, (2) a partially ordered structure of OT-16-DABA exists in solution under typical refolding conditions, and (3) structural constraints (presumably hydrophobic interactions) necessary for the formation of a chain-folding initiation site in RNase A are also present in the OT-16-DABA peptide in the absence of denaturant and are disrupted by Gdn-HCl.

It is generally thought that protein folding is initiated by short-range interactions that result in the formation of one or more chain-folding initiation sites (CFIS)[1] (Matheson & Scheraga, 1978; Wright et al., 1988; Montelione & Scheraga, 1989), formerly termed nucleation sites (Wetlaufer, 1973), within a polypeptide chain. Presumably these CFIS's reduce the amount of conformational space that the whole polypeptide needs to sample prior to folding. One model for identifying CFIS's is based on hydrophobic interactions that induce the formation of short hairpin-like conformations (Matheson & Scheraga, 1978). By computing the free energy of formation of such structures, Matheson and Scheraga (1978) identified several CFIS's in a group of proteins. In particular, several such sites were proposed for the folding of RNase A, the most stable of which was computed to consist of residues 106–118. By using an alternative model, based on the contact map of RNase S, Némethy and Scheraga (1979) identified six CFIS's (designated A–F) and came to similar conclusions about their location within the amino acid sequence.

† This work was supported by grants from the National Institutes of Health (GM-14312) and the National Science Foundation (DMB84-01811). Support was also received from the National Foundation for Cancer Research. J.M.B. was an NIH Postdoctoral Fellow (1987–1990).
* To whom correspondence should be addressed.
‡ Cornell University.
§ Bar-Ilan University.
‖ Weizmann Institute of Science.

[1] Abbreviations: Ac, acetyl; Acm, acetamidomethyl; CFIS, chain-folding initiation site; DABA, diaminobutyric acid; DCC, 1,3-dicyclohexylcarbodiimide; DCM, dichloromethane; DMA, dimethylamine; NHMe, *N*-methylamide; DMF, dimethylformamide; DNS, dansyl; EDTA, ethylenediaminetetraacetic acid; FMOC, *N*-(9-fluorenylmethoxycarbonyl)-; Gdn-HCl, guanidine-HCl; HEPES, 4-(2-hydroxyethyl)-1-piperazineethanesulfonic acid; NAA, naphthoxyacetic acid; NTSB, 2-nitro-5-thiolsulfobenzoate; RNase A, bovine pancreatic ribonuclease A (EC 3.1.4.22); OT-16, the 16th peptide isolated by chromatography from a tryptic (T) digest of oxidized (O) RNase A; D-OT-16, DNS-labeled OT-16-DABA; OT-16-N, OT-16-DABA labeled with NAA; D-OT-16-N, OT-16-DABA labeled with DNS and NAA; D-Lys-N, lysine labeled with DNS and NAA; O-t-Bu, *O-tert*-butyl; t-BOC, *tert*-butoxycarbonyl-; TEAA, triethylammonium acetate; TFA, trifluoroacetic acid; ET, energy transfer; NET, nonradiative energy transfer; NMR, nuclear magnetic resonance; EED, end-to-end distance.

0006-2960/91/0430-7680$02.50/0

The purpose of the present work was to determine whether the hydrophobic interactions among residues 106–118 of RNase A were strong enough to induce the formation of a folded structure in a peptide *fragment* containing these residues. Such an experimentally obtainable fragment is OT-16, which consists of the 20 C-terminal residues (105–124) of RNase A. This fragment can be prepared either by tryptic digestion of oxidized RNase A (Stimson et al., 1982) or by direct synthesis. It contains numerous nonpolar residues, one cysteine, a single amine (the N-terminal amine), and three carboxyl groups (Glu^{111}, Asp^{121}, and the C-terminal carboxyl group).[2] In addition, this region of RNase A exists as a hairpin-like antiparallel β-sheet structure containing a type VI β-turn at Gly^{112}-Asn^{113}-Pro^{114}-Tyr^{115} as identified from the crystal structure (Wlodawer et al., 1982).

The notion that peptides can be used to investigate CFIS's is based on five earlier studies of four different CFIS regions in RNase A that have examined peptide models. These peptides include (1) the N-terminal α-helix (CFIS A, residues 4–11), (2) the Cys^{58}–Cys^{72} peptide (CFIS D; residues 53–79), (3) the Ac-Tyr^{92}-Pro^{93}-Asn^{94}-NHMe peptide (CFIS E, residues 71–111), (4) the Ac-Asn^{113}-Pro^{114}-Tyr^{115}-NHMe peptide (CFIS F, residues 103–124), and (5) the OT-16 peptide (CFIS F, residues 103–124).

Peptides corresponding to the N-terminal α-helix of RNase A have been studied extensively in solution with the aid of circular dichroism and NMR (Silverman et al., 1972; Bierzynski et al., 1982; Kim et al., 1982; Mitchinson & Baldwin, 1986; Rico et al., 1986, 1987). The α-helix has been shown to be in dynamic equilibrium with the unfolded conformation. This equilibrium is temperature and pH dependent. Thus, the short-range interactions that direct the formation of a native-like CFIS structure are present in the peptide.

Studies of the Cys^{58}–Cys^{72} peptide (Milburn & Scheraga, 1988; Altmann & Scheraga, 1990) have shown that the loop with the native disulfide bond, Cys^{65}–Cys^{72}, is thermodynamically favored over the nonnative similar-size disulfide loop, Cys^{58}–Cys^{65}, providing an excellent example of enthalpic contributions to the formation of native structure by local interactions.

Peptides Ac-Tyr^{92}-Pro^{93}-Asn^{94}-NHMe and Ac-Asn^{113}-Pro^{114}-Tyr^{115}-NHMe, corresponding to fragments with type VI β-turns (with *cis*-proline) in CFIS E and F, respectively, have been studied by NMR and X-ray crystallographic methods (Stimson et al., 1982; Montelione et al., 1984). The results have shown that these short peptides have little preference for the native *cis*-proline conformation that exists in the RNase A crystal structure (Wlodawer et al., 1982). Thus, while these tripeptides are folded, the local interactions are not sufficient to lead to the native cis conformation of the proline residue in these peptides.

Finally, tyrosine fluorescence lifetime and nuclear magnetic resonance (NMR) experiments on OT-16, CFIS F, have indicated that this peptide exists in two or more conformations that arise from interactions other than cis/trans isomerization about the peptide bond preceding Pro^{114} (Haas et al., 1987). Presumably, a dynamic equilibrium exists between the native and unfolded conformations. The present paper addresses the hypothesis that the short-range interactions present in OT-16, aided in particular by the type VI β-turn located at Gly^{112}-Asn^{113}-Pro^{114}-Tyr^{115}, drive the formation of a compact structure in the OT-16 region of RNase A.

[2] The numbering system is based on the amino acid sequence of RNase A.

In this study, we have investigated the feasibility of monitoring conformational changes in OT-16 by using a doubly labeled molecule in conjunction with nonradiative energy transfer (NET) experiments. The design of NET experiments is based on numerous criteria. This paper focuses on the selection of the probes, the solid-phase synthesis of the OT-16-DABA species, the stoichiometric labeling of OT-16-DABA, the purification of the necessary derivatized materials, the type of analysis required for studying this dynamic system, and the conformation of OT-16 under a variety of solution conditions.

Experimental Procedures

Nonradiative Energy Transfer (Fairclough & Cantor, 1978). Nonradiative energy transfer is a process in which the electronic excitation energy from a donor probe is transferred nonradiatively to an acceptor probe by means of dipole–dipole interactions. The rate of energy transfer (k_t) depends on a number of factors:

$$k_t = (8.79 \times 10^{-5})\kappa^2 n^{-4} Q_D J_{DA} \tau_D^{-1} r^{-6} \quad s^{-1} \qquad (1)$$

where κ^2 is a parameter that relates the orientation of the emission dipole of the donor and the excitation dipole of the acceptor, n is the refractive index of the medium, Q_D is the quantum yield of the donor, J_{DA} is the overlap integral arising from the corrected donor fluorescence emission and acceptor molar extinction coefficient profiles, τ_D is the fluorescence lifetime of the donor, r is the interprobe distance between the two dipoles, and the numerical factor is required to express k_t in s^{-1}. The dependence of k_t on r makes it possible to determine conformational properties of molecular systems.

Fluorescence Intensity Measurements (Haas, 1986). Transfer efficiencies were determined by monitoring the fluorescence excitation spectrum of the acceptor at an emission wavelength of 555 nm (emission slit width = 20 nm) in the absence and presence of the donor. In the presence of the donor, the fluorescence of the acceptor is enhanced by transfer of excitation energy from the donor. Acceptor excitation spectra (200–400 nm; slit width = 4 nm) of three samples were recorded routinely: (1) D-OT-16 (acceptor only, the 0% ET reference), (2) D-OT-16-N (donor- and acceptor-labeled peptide, the ET experiment), and (3) D-Lys-N (donor and acceptor attached to a single lysine, the 100% ET reference). The spectra were normalized over the wavelength range of 340–400 nm, in which only the DNS is excited but not the NAA. It is also important to note that the fluorescence of NAA above 400 nm is negligibly small and does not contribute to the emission profile of DNS at 555 nm.

The efficiency of energy transfer was determined by calculating the areas between the normalized excitation spectra of the sample D-OT-16-N, or D-Lys-N (the 100% transfer reference), and that of D-OT-16 (the 0% transfer reference). The difference spectra were fit with a spline (de Boor, 1978), and the areas under the resulting curves were calculated by analytical integration. These spline fits were extremely accurate with negligible residuals. The integration was carried out over a limited range, from 296 to 330 nm. The lower limit was selected to eliminate any possible contribution from tyrosine excitation.

All fluorescence intensity measurements were made on a Perkin-Elmer MPF-44B fluorescence spectrophotometer in the energy mode. A 360-nm cut-off filter was placed in the emission pathway to eliminate interference from scattered light from the sample. Homemade quartz microcuvettes, 5 mm × 5 mm cross section (i.d.), with a 35 mm (length) × 5 mm (O.D) quartz tube extension were used in the measurements.

A neoprene septum was attached to prevent evaporation. All samples were diluted to nearly identical concentrations, and absorbances were below 0.05 AU at the wavelength of excitation. Quinine sulfate (1 μM solution in 1 M H_2SO_4) was used as a standard for monitoring drift of the instrument by measuring the fluorescence of the quinine sulfate standard before and after each series of experiments. No appreciable drift was observed. Fluorescence spectra were corrected for fluorescent impurities with the aid of blanks consisting of the appropriate buffer and denaturants. These corrections were made in all cases. All spectra were digitized by a custom built analogue-to-digital converter and stored on a Prime 750 minicomputer. A FORTRAN 77 program was used to process the routines for concentration correction, normalization, and calculation of difference spectra. Spline and integration routines on the Prime 750 were used to determine the appropriate values of the areas.

Lifetime Measurements (Fairclough & Cantor, 1978). Donor fluorescence lifetime measurements were made in the presence and absence of the acceptor. The average transfer efficiency was calculated form these decay profiles. Time-dependent fluorescence decay measurements were made on an Edinburgh Instruments Ltd. (Edinburgh, Scotland) 199DS fluorescence lifetime spectrometer. Samples were excited by using a nanosecond nitrogen flashlamp, and the decaying fluorescent emissions were collected by a photomultiplier operated in a single photon counting regime (O'Conner & Phillips, 1984a). Both excitation (316 nm) and emission [345 nm (donor) or 555 nm (acceptor)] bands were selected by monochromators. Correction for scattered light and background fluorescence were made with the technique of Haas et al. (1978b). The data were collected with a multichannel analyzer and subsequently stored on an AST 80286 microcomputer.

Average Transfer Efficiencies. Efficiencies of transfer were determined for double-exponential decay profiles by using the lifetime values calculated by the least-squares analyses of the observed decay curves (Grinvald & Steinberg, 1974; O'Conner & Phillips, 1984b; Imhof, 1987) and calculating a weighted-average lifetime, according to

$$\langle \tau \rangle = \sum_{i=1}^{n} \alpha_i \tau_i / \sum_{i=1}^{n} \alpha_i \qquad (2)$$

where n is the number of exponentials used to fit the fluorescence decay curve, and α_i and τ_i are the amplitude and lifetime of the ith component.

Analysis of Dynamic Distance Distribution (Haas, 1986; Beechem & Haas, 1989). Distributions of distances between donor and acceptor were determined from the lifetime measurements by using a global analysis of sets of four experiments: (1) donor decay in absence of an acceptor, (2) donor decay in the presence of acceptor, (3) acceptor decay in the absence of donor, and (4) acceptor decay in the presence of donor (Beechem & Haas, 1989). A calculated decay curve $I_c(t)$ was generated from the expression

$$I_c(t) = k \int_a^{r_m} N_o(r) \bar{N}(r,t)\, dr \qquad (3)$$

where a is the limiting short distance of closet approach of the chain ends, r_m is the interprobe distance of the fully extended conformation, k is a proportionality constant, $N_o(r)$ is the equilibrium interprobe distance distribution, and $\bar{N}(r,t)$ is the time-dependent normalized distribution of interprobe distances in the population of molecules with an excited donor. The calculated decay curve was then convoluted iteratively with the lamp profile to reconstitute the observed decay profile.

The equilibrium interprobe distance distribution was modeled by a skewed Gaussian (Edwards, 1965) with adjustable parameters according to

$$N_o(r) = 4\pi c r^2 \exp[-a(r-b)^2] \qquad (4)$$

where r is the distance in Å, a and b are adjustable parameters and $4\pi c$ is a normalization constant. $\bar{N}(r,t)$ was obtained as a solution of a second-order partial differential equation, eq 5, which contains terms for spontaneous fluorescence decay, energy transfer, and diffusion:

$$\frac{\partial \bar{N}(r,t)}{\partial t} = \left\{ \frac{1}{\tau_D} \left[1 + \left(\frac{R_o}{r} \right)^6 \right] \right\} \bar{N}(r,t) + \frac{1}{N_o(r)} \frac{\partial}{\partial r} \left[N_o(r) D \frac{\partial \bar{N}(r,t)}{\partial r} \right] \qquad (5)$$

where $\bar{N}(r,t) = N^*(r,t)/N_o(r)$ in which $N^*(r,t)$ is the interprobe distance distribution of the ensemble of molecules with an excited donor at time t after excitation [where $N^*(r,0) = N_o(r)$] and D is the diffusion coefficient of the two probes (relative to one another) (Haas et al., 1978b; Beechem & Haas, 1989). Global analysis of all four decay curves allows for simultaneous determination of $N_o(r)$ and D (Beechem & Haas, 1989).

Overlap Integrals, Quantum Yields, Refractive Indices, and R_o (Fairclough & Cantor, 1978). The overlap integral, J_{DA} (eq 1), was calculated for each set of conditions using the corrected emission spectrum of the donor-labeled peptide and the molar extinction coefficient spectrum of the acceptor-labeled peptide. The relative quantum yields of OT-16-N, Q_D (eq 1), were estimated from lifetime measurements by using the comparative method of Chen et al. (1969). This technique was previously employed to determine the quantum yield of NAA by using zone-refined naphthalene as a standard (McWherter et al., 1986).

Refractive indices, n (eq 1), were determined at the sodium D line by using an Abbé refractometer (Bausch & Lomb, Rochester, NY). The refractive indices were essentially independent of wavelength in the range used in this study and were used in the calculation of the Förster critical distance, R_o. The concentration of Gdn-HCl was also determined from refractive index measurements (Nozaki, 1972).

The mutual orientation factor, κ^2 (eq 1), of the emission dipole of the donor and excitation dipole of the acceptor was assumed to be $^2/_3$. This is a valid assumption in probe systems that exhibit low intrinsic polarization and dipole orientation that is randomized by rotational diffusion prior to energy transfer. The probes used in this study have a low intrinsic polarization (Anderson, 1969; McWherter et al., 1986), which implies that their electronic transitions are of mixed polarization (Haas, et al., 1978a); this latter property reduces the error introduced by the assumption that $\kappa^2 = {}^2/_3$ to less than 10% (Haas et al., 1978a).

Corrected Fluorescence Emission Spectra (Lakowicz, 1983). Emission spectra were corrected by employing a Perkin-Elmer DCSU-2 spectral correction unit in conjunction with the Perkin-Elmer MPF-44B fluorescence spectrophotometer. All data were digitized by a custom-made analogue-to-digital converter and stored on a Prime 750 minicomputer.

Extinction Coefficients. Extinction coefficient profiles of OT-16-N and D-OT-16 were obtained from ultraviolet absorption spectra recorded on a modified Cary 14, digitized by means of a custom-made analogue-to-digital converter, and stored on a Prime 750 minicomputer. Concentrations of samples were determined by quantitative amino acid analysis

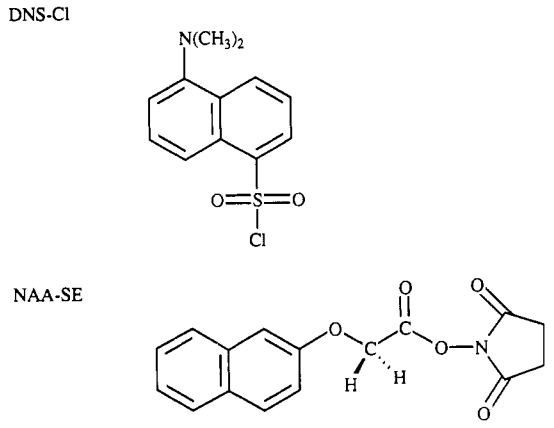

FIGURE 1: DNS-Cl, 5-(dimethylamino)-L-naphthalene sulfonyl chloride (dansyl chloride); NAA-SE, 2-naphthoxyacetic acid, *N*-hydroxysuccinimide ester.

on a Waters Pico-Tag system (Milford, MA) at the Biotechnology Analytical and Synthesis Facility of Cornell University (Ithaca, NY).

Selection of Probes. The probes selected for this study (Figure 1) were dimethylaminonaphthalene sulfonyl (DNS) as the acceptor and naphthoxyacetic acid (NAA) as the donor. The naphthoxyacetic acid was a suitable choice as the donor because it exhibits a monoexponential lifetime decay profile and a high quantum yield (McWherter et al., 1986); it can be excited with a nitrogen flash lamp (316 nm) and exhibits extensive overlap between the donor emission spectrum and acceptor excitation spectrum.

Materials. The FMOC- and BOC- orthogonally protected amino acids for peptide synthesis were obtained from MilliGen (Milford, MA). DABA, DCM, DMA, bicine, NAA *N*-hydroxysuccinimide ester, and dansyl chloride were obtained from Aldrich Chemical Co., Milwaukee, WI. TFA was purchased from Burdick and Jackson Laboratories, Inc. (Muskegon, MI). TEAA was obtained from Pierce Chemical Co. (Rockford, IL). HEPES buffer was purchased from Sigma Chemical Co. (St. Louis, MO). DMF, from Aldrich Chemical Co., was distilled under reduced pressure in a nitrogen atmosphere and stored over 3-Å molecular sieves under a nitrogen atmosphere. Prior to use, nitrogen was bubbled through the DMF to remove volatile amines.

Preparation of α-FMOC-γ-t-BOC-Diaminobutyric Acid. The synthesis of the modified OT-16 species with DABA at the C-terminus required the initial synthesis of α-FMOC-γ-t-BOC-diaminobutyric acid. First, the copper salt of DABA was prepared by dissolving L-α,γ-DABA dihydrochloride (1.90 g, 9.95 mmol) in boiling water (15 mL) and adding copper carbonate (2 g, 18 mmol) with vigorous stirring (Moroder et al., 1976). Excess copper carbonate was removed from the soluble copper salt of diaminobutyric acid by filtering through a sintered glass funnel; the precipitate was subsequently washed with 5 mL of hot water, and the washings were added to the filtrate.

The second step was the synthesis of γ-t-BOC-DABA cupric salt. The blue filtrate of the copper salt of DABA (~20 mL) was chilled in an ice bath. The solution was made basic by the addition of sodium bicarbonate (0.84 g, 10 mmol). The labeling of the γ-amine was initiated by the addition of di-*tert*-butyl dicarbonate (2.4 g, 11 mmol) dissolved in dioxane (25 mL) with vigorous stirring (Moroder et al., 1976). The reaction proceeded for 4 h at room temperature. The γ-t-BOC-DABA cupric salt precipitated upon formation and was isolated by filtration on a sintered glass funnel. The precipitate was washed successively with water, acetone, and ether. The yield was 1.25 g (5 mmol).

The third step involved the removal of the copper from the product. The free amino acid, γ-t-BOC-DABA, was obtained by bubbling hydrogen sulfide through a stirred suspension of the cupric salt of γ-t-BOC-DABA in water (50 mL) for 30 min at room temperature. At the end of this period, the mixture was heated to boiling and filtered hot through a sintered glass funnel. The product, in the filtrate, was lyophilized.

The final step in the synthesis (Sigler et al., 1983) yielded the desired α-FMOC-γ-t-BOC-DABA. The γ-t-BOC-DABA (0.84 g, 3.9 mmol) was dissolved in 5 mL of a 10% (w/v) aqueous solution of sodium carbonate (0.45 g, 4.3 mmol). This mixture was added to a solution of 9-fluorenylmethylsuccinimidyl carbonate (1.05 g, 3.1 mmol) in dioxane (5 mL) with vigorous stirring. Water was added until the solution was clear. The reaction proceeded for 12 h at room temperature. The reaction mixture was then diluted to 50 mL with water and extracted with ethyl acetate. The original water fraction was acidified to pH 2 with sodium hydrogen sulfite and extracted with ethyl acetate. The collected ethyl acetate fractions were washed with a 2.5% solution of sodium hydrogen sulfite (2×) and water (2×) in attempt to extract any residual product, the sodium salt of α-FMOC-γ-t-BOC-DABA, into the aqueous phase. Despite the successive attempts at extraction, the sodium salt of α-FMOC-γ-t-BOC-DABA remained in the ethyl acetate fraction. The ethyl acetate fraction was recovered and the product purified by flash chromatography (Still et al., 1978) as described below.

The product was identified in the ethyl acetate extract by TLC in a solvent system of toluene/acetic acid (7:3), R_f = 0.45. TLC and NMR showed that the product was not pure. The α-FMOC-γ-t-BOC-DABA was purified by using flash chromatography in a solvent system of chloroform/acetic acid (20:1). The bed was Silica gel 60 with a particle size of 0.04–0.063 mm. The first 200 mL of eluant were collected in four 50-mL fractions. The α-FMOC-γ-t-BOC-DABA eluted in a broad band between fractions 20 and 65, each fraction being equivalent to ~15 mL. TLC analysis of the peak revealed only one product in each fraction spanning the peak. The TLC's were developed in acetic acid/butanol/water (1:3:1), R_f = 0.82, and chloroform/acetic acid (20:1), R_f = 0.11, and the products were identified by UV irradiation. The fractions were pooled, the acetic acid extracted into water (5×), the chloroform solution was dried with sodium sulfate, and the solvent was evaporated under reduced pressure to yield 1.26 g. The NMR spectrum identified: 9H [singlet, 1.35 ppm, t-BOC-$(CH_3)_3$], 1H (multiplet, 1.68 ppm, β-CH_2), 1H (multiplet, 1.82 ppm, β-CH_2), 2H (multiplet, 2.9–3.05 ppm, γ-CH_2), 1H (multiplet, 3.95 ppm, α-CH), 3H (multiplet, 4.25 ppm, -CH_2- of the FMOC group), 1H (triplet, 6.82 ppm, α-NH), and 9H (multiplet, 7.25–7.45 ppm; multiplet, 7.6–7.8 ppm; doublet, 7.9 ppm, FMOC protons). The authenticity of this material was further confirmed by mass spectral data of synthesized peptides containing this residue.

Solid-Phase Synthesis of OT-16-DABA. A custom PepSyn KA derivatized resin (MilliGen, Bedford, MA) was used for the synthesis of the modified OT-16 species with DABA at the C-terminus. The modified resin support, PepSyn KA-α-FMOC-γ-t-BOC-DABA, with the carboxyl group of the DABA linked to the resin by an ester linkage with 4-hydroxymethylphenoxyacetic acid, was synthesized according to the MilliGen technical note 4.30 (1987). The symmetrical anhydride of α-FMOC-γ-t-BOC-DABA was produced by mixing dicyclohexylcarbodiimide (0.233 g, 1.08 mmol) with

α-FMOC-γ-t-BOC-DABA (0.95 g, 2.16 mmol) in a solution of DCM (20 mL) and DMF (5 mL) for 20 min at room temperature. The dicyclohexylurea was filtered off with a sintered glass filter. The filtrate with symmetrical anhydride product was evaporated under reduced pressure and dissolved in a minimum volume of DMF (5 mL) to which 2 g of the PepSyn KA resin was then added. The coupling of α-FMOC-γ-t-BOC-DABA to the resin was initiated by the addition of dimethylaminopyridine (0.022 g, 0.18 mmol). The mixture was stirred manually at room temperature and allowed to react for 2 h. The resin was washed on a sintered glass funnel with DMF (4 × 10 mL), DCM (4 ×10 mL), methanol (2 × 10 mL), and finally with DCM (2 × 10 mL). The resin, KA-α-FMOC-γ-t-BOC-DABA, was dried in vacuum over phosphorus pentoxide.

The peptide was synthesized at the Biotechnology Analytical and Synthesis Facility at Cornell University (Ithaca, NY) on a MilliGen 9050 PepSynthesizer (MilliGen, Bedford, MA) according to the MilliGen technical note 3.10 (1987). The KA-α-FMOC-γ-t-BOC-DABA resin (1.1 g) was added to the reaction column, and the peptide was synthesized with activated esters of blocked amino acids supplied by MilliGen. The orthogonally blocked amino acids included FMOC-L-His-(BOC), FMOC-L-Asp(O-t-Bu), FMOC-L-Glu(O-t-Bu), FMOC-L-Ser(O-t-Bu), FMOC-L-Tyr(O-t-Bu), and FMOC-L-Cys(Acm). Standard coupling times of 60 min were used with exceptions at positions Val^{12}, Ile^{3}, Ile^{2}, and His^{1} for which 90-min coupling times were used. The N-terminal FMOC group was not removed at the end of the synthesis in order to facilitate labeling with the fluorescent probes at a later stage.

Cleavage of OT-16-DABA from PepSyn KA Resin. The peptide, either the N-terminal protected or the N-terminal deprotected peptide, was cleaved from the resin according to MilliGen technical note 5.21 (1987). Routinely, the resin (30 mg) was placed in a polypropylene tube, and the peptide was cleaved from the resin with TFA (0.9 mL) neat. Thiophenol (0.1 mL or 10%) was added to the reaction mixture as a scavenger for carbocations and other reactive species that are generated during the synthesis. The reaction time was 2 h at room temperature. The reaction mixture was centrifuged, and the TFA solution was decanted. The resin was washed with TFA (6 × 1 mL). The TFA extracts were combined and dried under reduced pressure. The dried peptide residue was washed with ether to remove any of the scavenger reagent. The ether-suspended insoluble peptide was isolated by centrifugation, dissolved in water, and lyophilized. The isolated peptide was free of all acid-labile protecting groups, including the cysteine, with the exception of the N-terminal FMOC group. When it was desired to remove the FMOC group, the resin was treated with a mixture of DMA (15–20%) in DMF (1 mL).

Sulfonation of OT-16-DABA. The free thiol on the deprotected peptide was sulfonated according to the procedure of Thannhauser et al., (1985). The lyophilized peptide (~1 mg from 30 mg resin) was dissolved in 120 μL of buffer (0.3 M Na_2SO_3, 0.2 M Tris-HCl, 6M Gdn-HCl, 3 mM EDTA, pH 8.5). After 10 min, 80 μL of disodium 2-nitro-5-thiosulfobenzoate stock solution (50 mM NTSB, 1 M Na_2SO_3) was added. The reaction was allowed to continue for 20 min at room temperature. The peptide was then desalted by using reverse-phase chromatography in a water/TFA solvent system. The peptide was eluted by using an acetonitrile gradient as described in the reverse-phase HPLC section.

Preparation of D-OT-16. The N-terminus of the OT-16 peptide was labeled with dansyl chloride while still attached to the resin. This approach provided exclusive stoichiometric labeling of the N-terminus because of the presence of the acid-labile blocking groups protecting the two histidines, cysteine, DABA, and tyrosine. These latter groups could otherwise be labeled by dansyl chloride. The N-terminal FMOC group was first removed from the peptide attached to the resin (50 mg) by using DMF/DMA (20%) solution (1 mL) at room temperature for 4 h. The N-terminal amine (~3.5 μmol)[3] was then labeled with dansyl chloride (1.75 mg, 6.5 μmol) in a solution of DMF (1 mL)/diisopropylethylamine (0.68 μL, 3.9 μmol). The reaction proceeded for 4 h at room temperature. The resin was then washed with DMF (3 × 5 mL), acetone (3 × 5 mL), and DCM (3 × 5 mL) to remove any unreacted dansyl chloride and was subsequently dried under vacuum. The peptide, with dansyl label, was cleaved from the resin, and the free thiol was sulfonated as described above. The sulfonated D-OT-16 peptide was isolated by reverse-phase chromatography, as described above. The peptide was characterized by amino acid analysis and electrospray mass spectrometry.

Preparation of D-OT-16-N. A portion of the sulfonated D-OT-16 was used for labeling the free γ-amine of DABA with NAA *N*-hydroxysuccinimide ester. A stock solution (6 mM) was prepared by dissolving 2 mg (6 μmol) of NAA *N*-hydroxysuccinimide ester in DMF (1 mL). The sulfonated D-OT-16 (1.5 mg, 0.61 μmol) was dissolved in 128 μL of HEPES buffer (0.20 M HEPES, 10 mM EDTA, pH 8.0). The reaction was initiated by the addition of NAA *N*-hydroxysuccinimide ester (128 μL of stock solution, 0.73 μmol), and the reaction mixture was stirred at room temperature for 12 h. The product was then isolated by using reverse-phase chromatography, as described below.

Preparation of OT-16-N. The synthesis of sulfonated OT-16-N was facilitated by labeling the γ-amine of DABA with the N-terminus protected with the FMOC group. The labeling process was essentially the reverse of the procedure used in the labeling of the OT-16 at the N-terminus. The FMOC-OT-16-DABA peptide was cleaved from the resin (as described above for D-OT-16), sulfonated, and purified by reverse-phase HPLC, as described below. The γ-amine of DABA was labeled, as described above for D-OT-16-N.

Reverse-Phase HPLC. All of the peptides and derivatized peptides were purified by reverse-phase HPLC using an RCM-100 radial compression system (Waters, Milford, MA) and a 0.8 cm × 10 cm column packed with NOVA-PAK C-18 resin with a 4 μm particle size. The underivatized sulfonated OT-16-DABA and monoderivatized OT-16-DABA species (FMOC-OT-16-DABA, D-OT-16, and OT-16-N) were chromatographed on a reverse-phase column using solvent systems A (0.09% TFA/water) and B (0.09% TFA/9.91% water/90% acetonitrile) (Figure 2). The column was equilibrated with water/acetonitrile/TFA (94.91%:5.00%:0.09%) solution and maintained under these conditions for the first 5 min of the run, at a flow rate of 1.00 mL/min. The peptides were eluted with a linear acetonitrile gradient from 5 to 50% over a 20-min period. The concentration of solvent B was maintained at 50% for 5 min prior to the 5-min gradient change to the initial conditions.

The doubly labeled species, D-OT-16-N and D-Lys-N, were chromatographed on a reverse-phase column using solvent systems A (0.1 N TEAA/95.0% water/5.0% acetonitrile/pH 7.0) and B (0.1 N TEAA/40.0% water/60.0% acetonitrile/pH 7.0) (Figure 2). The column was equilibrated with water/

[3] Based upon the number of attachment sites per particle of resin (0.065 mequiv/g).

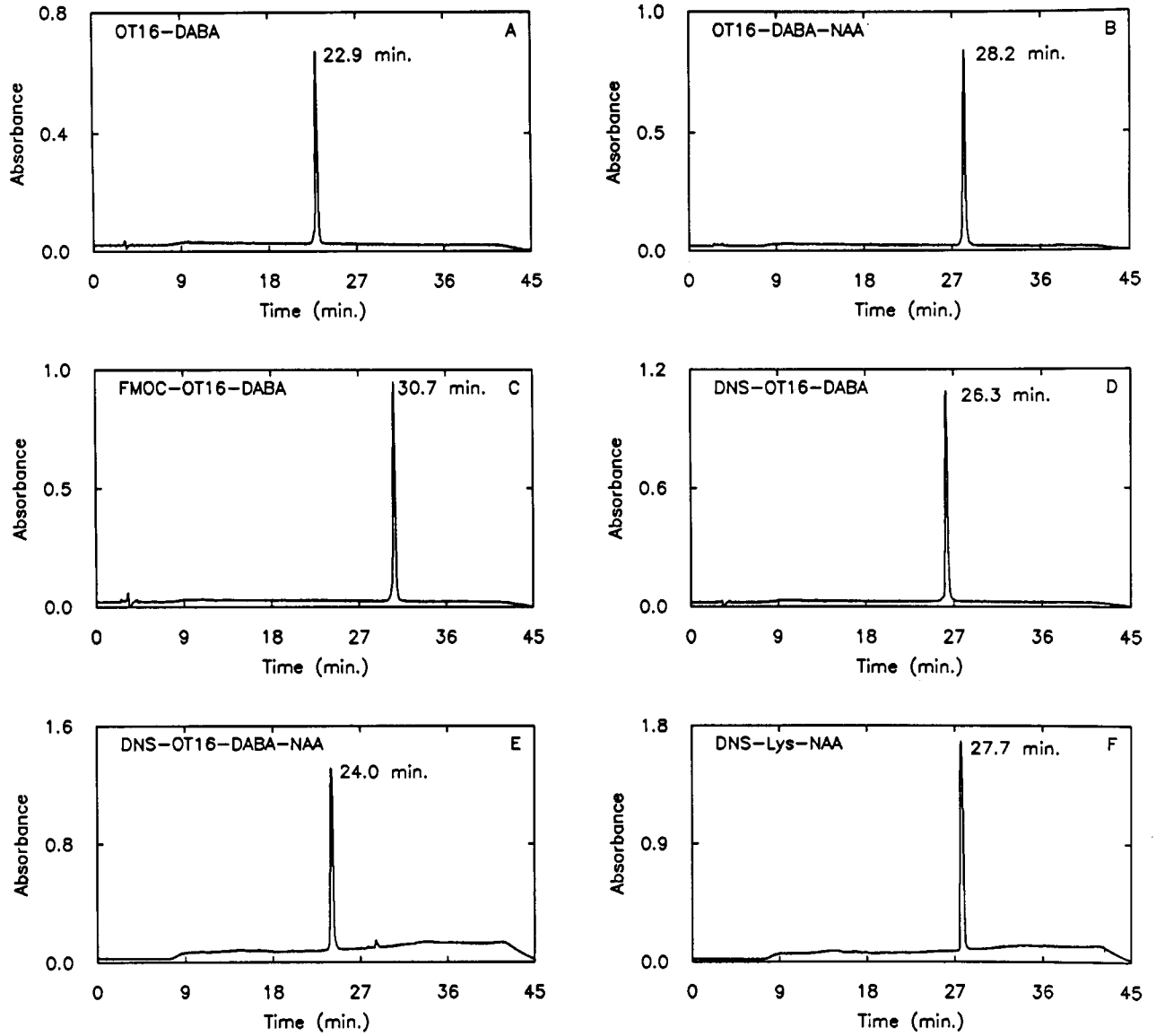

FIGURE 2: Reverse-phase high-performance liquid chromatography of sulfonated species. The samples were chromatographed as described under Experimental Procedures. The underivatized and monoderivatized peptides were isolated in water/TFA solution with an acetonitrile gradient and effluent monitored at 210 nm. The doubly labeled peptides were isolated in water/TEAA solution with an acetonitrile gradient and effluent monitored at 223 nm. Elution times are listed for each sample.

acetonitrile/TEAA (95.0%:5.00%:0.1 N) solution and maintained under these conditions for the first 5 min of the run, at a flow rate of 1.00 mL/min. The peptides were eluted with a linear acetonitrile gradient from 5 to 60% over a 20-min period. The concentration of solvent B was maintained at 60% for 5 min prior to the 5-min gradient change to the initial conditions.

All runs were carried out on an LKB 2249 Gradient Pump system (LKB, Sweden) equipped with a Rheodyne 7125 injector (Rheodyne, CA) and a 2140 rapid spectral detector (LKB, Sweden). The data from the diode array detector were digitized and transferred to a CompuAdd 80286 microcomputer.

Amino Acid Analysis. Amino acid analyses were carried out at the Biotechnology Analytical and Synthesis Facility at Cornell University (Ithaca, NY). Peptides were subjected to gas-phase hydrolysis with HCl, the amino acids precolumn derivatized with phenylisothiocyanate, and the phenylisothiocarbamyl derivatives analyzed by using reverse-phase chromatography (Heinrikson & Meredith, 1984). The amount of amino acid recovered per residue was determined from linear least-squares analyses.

Amino Acid Sequence Analysis. The amino acid sequence analyses were carried out at the Biotechnology Analytical and Synthesis Facility at Cornell University (Ithaca, NY). The sequence of the synthesized sulfonated OT-16-DABA was determined by using an Applied Biosystems, Inc. (Foster City, CA) 470A gas-phase protein sequencer, using Edman degradation chemistry (Hunkapiller et al., 1986).

Pneumatic-Assisted Electrospray Mass Spectrometry. The electrospray mass spectrometry was carried out at the Equine Drug Testing Facility at Cornell University (Ithaca, NY). The molecular weights of the sulfonated OT-16-DABA and sulfonated D-OT-16 were determined on a Sciex mass spectrometer equipped with a pneumatic-assisted electrospray unit for the soft ionization of the peptides (Covey et al., 1988). Positive ion mode spectra were determined in formic acid solutions. Negative ion mode analyses required the presence of the sulfonated thiol and that the peptides be solubilized in a TEAA buffer, pH 7.0.

RESULTS

Solid-Phase Synthesis. Potential problems in the synthesis of OT-16, arising from the presence of several carboxyl groups

Table I: Amino Acid Analysis of OT-16-DABA

amino acid	theoretical[a]	exptl[b]	amino acid	theoretical[a]	exptl[b]
Asx	2	2.2	Tyr	1	1.0
Glx	1	1.1	Val	4	3.7
Ser	1	1.1	Cys	1	0.8
Gly	1	1.3	Ile	2	1.4
His	2	1.7	Phe	1	0.9
Ala	2	1.8	DABA	1	1.0
Pro	2	1.9			

[a] Theoretical amounts of amino acids based on amino acid sequence. [b] Experimentally determined amounts of amino acids determined by using the Waters Pico-Tag system (Bedford, MA).

in OT-16, were circumvented by using a solid-phase synthetic approach coupled with an orthogonal blocking scheme. OT-16 was synthesized with an additional amino acid, DABA, at the C-terminus of the peptide. A small portion of the resin, 15 mg, was deprotected, and the modified peptide, OT-16-DABA, was purified to homogeneity by reverse-phase chromatography (Figure 2). The purified OT-16-DABA was characterized by amino acid analysis, amino acid sequence analysis, and electrospray mass spectrometry.

The amino acid analysis results (Table I) indicate that the composition of the peptide is that of the target peptide, within 10% error. Glycine is high due to contamination by the buffer. Histidine, valine, and isoleucine are low because these residues are present in a His^{105}-Ile^{106}-Ile^{107}-Val^{108} sequence, which is difficult to hydrolyze completely without destroying other amino acids. The sequence of the target peptide was confirmed by amino acid sequence analysis to be HIIVACEGN-PYVPVHFDASV. The C-terminal amino acid, DABA, was not identified since the last amino acid in a sequence run is washed out of the system. The amino acid analysis coupled with the sequence data identifies the C-terminus of the peptide as a DABA. The measured average moleclar weight of the purified target peptide, as determined by electrospray mass spectrometry, was 2346.3 Da, which is in close agreement with the calculated average molecular weight of 2347.1 Da.

Synthesis of Peptide Derivatives. The DABA provided a side chain with a γ-amino group for the coupling of NAA to the C-terminal region of the peptide. Stoichiometric labeling of the sulfonated peptide was achieved by orthogonally protecting the two amino groups on the newly modified peptide (see Experimental Procedures). The N-terminal amino group was protected with a base-labile protecting group, FMOC, and the γ-amino group of DABA side chain, located at the C-terminus, was protected with an acid-labile protecting group, t-BOC. This protecting scheme allowed for the systematic deprotection of the desired amino group for stoichiometric labeling.

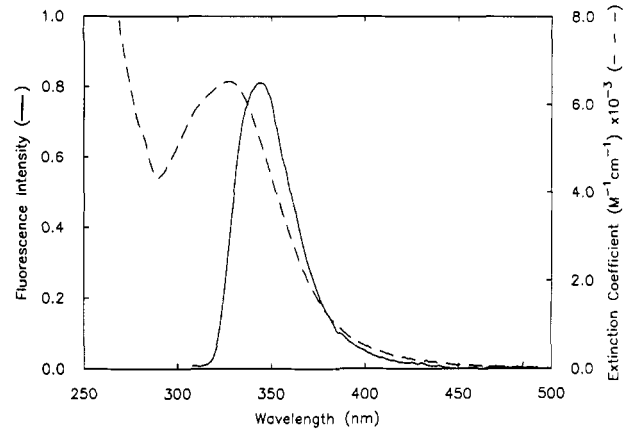

FIGURE 3: Corrected fluorescence emission spectrum of OT-16-N and absorption spectrum of D-OT-16. The emission spectrum of OT-16-N has extensive overlap with the absorption spectrum of D-OT-16, thereby satisfying the requirement for energy transfer. The corrected fluorescence spectrum was determined with bandwidths of 10 and 6 nm for emission and excitation, respectively, at an excitation wavelength of 260 nm and a concentration of OT-16-N of 0.23 μM. The absorption spectrum was determined at a concentration of D-OT-16 of 30 μM.

All three derivatized species (D-OT-16, D-OT-16-N, and OT-16-N) were purified to homogeneity by reverse-phase chromatography (Figure 2). Isolation of the appropriately derivatized peptides was confirmed by amino acid analysis, determination of the extinction coefficients, and fluorescence spectral properties. Multiply dansylated species of OT-16-DABA were not obtained because the DABA, tyrosine, cysteine, and two histidine side chains were protected with acid-labile groups during the labeling procedure. Thus, only the N-terminal amine was available for labeling with dansyl chloride. To verify that only monodansylated material was produced, the sample was submitted for analysis by mass spectrometry. This analysis of D-OT-16 yielded a mass of 2579.2 Da, which is within 1 Da of the calculated average mass. The γ-amine of DABA was labeled with the more selective reagent NAA *N*-hydroxysuccinimide ester after sulfonation of the free thiol and with the N-terminal amine either protected or labeled. The labeling sequence was therefore crucial for the stoichiometric labeling of sulfonated OT-16-DABA.

Table II: Energy Transfer and Related Results in the Absence of 6 M Gdn-HCl

sample[a]	temp[b] (°C)	τ[c] (ns)	SD[d]	χ^2[e]	n[f]	J(× 10^{15}) (M^{-1} cm^3)	Q_d	R_0 (Å)	% $E(I)$[g]	% $E(\tau)$[h]	$r(I)$[i] (Å)	$r(\tau)$[j] (Å)
D	1.5	11.46	0.02	1.34								
DA	1.5	7.27[k]	0.19	1.27	1.3355	5.68	0.52	28.6	28	37	33.5	31.3
D	20	10.41	0.01	1.27								
DA	20	5.60[k]	0.32	1.15	1.3345	5.71	0.48	28.2	37	46	30.8	29.0
D	40	9.15	0.01	1.16								
DA	40	4.99[k]	0.12	1.48	1.3323	5.63	0.42	27.6	43	45	29.0	28.5
D	60	7.99	0.01	1.14								
DA	60	4.10[k]	0.09	1.31	1.3299	5.79	0.36	27.0	49	49	27.2	27.2

[a] D = OT-16-N; DA = D-OT-16-N. [b] Conditions used were as follows: 50 mM bicine and 1 mM EDTA, pH 8.0. [c] Results of least-squares fit of the fluorescence decay kinetics with the equation $F(t) = \alpha e^{-t/\tau}$, where $F(t)$ is the observed fluorescence decay, α is the amplitude, and τ is the lifetime. The lifetime and amplitude data were determined by using a nonlinear least-squares iterative reconvolution technique supplied by Edinburgh Instruments Ltd. (Imhof, 1987). [d] Standard deviation of the lifetime values. [e] Chi-squared analysis of the residuals. Chi-squared values between 1 and 1.5 are acceptable (O'Conner & Phillips, 1984c). [f] Refractive index at the sodium line. [g] Percent of energy transferred as determined by steady-state measurements. [h] Percent of energy transferred as determined by fluorescence lifetime measurements. [i] Apparent interchromophore distance as determined from steady-state measurements, assuming a unique interprobe distance. [j] Apparent interchromophore distance as determined from fluorescence lifetime measurements, assuming a unique interprobe distance. [k] Average lifetimes where $\langle\tau\rangle = \sum\alpha_i\tau_i/\sum\alpha_i$ where $i = 1$ in the absence of DNS and $i = 2$ in the presence of DNS.

Table III: Energy Transfer and Related Results in the Presence of 6 M Gdn-HCl

sample[a]	temp[b] (°C)	τ[c] (ns)	SD[d]	χ^2[e]	n[f]	$J(\times 10^{15})$ (M^{-1} cm^3)	Q_d	R_0 (Å)	% $E(I)$[g]	% $E(\tau)$[h]	$r(I)$[i] (Å)	$r(\tau)$[j] (Å)
D	1.5[d]	8.04	0.01	1.44								
DA	1.5	5.76[k]	0.30	1.29	1.4392	5.61	0.37	25.6	28	28	30.0	30.0
D	20[d]	7.57	0.01	1.64								
DA	20	5.34[k]	0.35	1.59	1.4362	5.55	0.35	25.4	31	29	29.0	29.5
D	40[d]	7.06	0.01	1.44								
DA	40	4.48[k]	0.25	1.26	1.4334	5.70	0.32	25.2	31	37	29.0	27.5
D	60[d]	6.57	0.01	1.38								
DA	60	3.82[k]	0.32	1.13	1.4293	5.67	0.30	24.9	38	42	27.0	26.3

[a] D = OT-16-N; DA = D-OT-16-N. [b] Conditions used were as follows: 50 mM bicine, 1 mM EDTA and 6 M Gdn-HCl, pH 8.0. [c] Results of least-squares fit of the fluorescence decay kinetics with the equation $F(t) = \alpha e^{-t/\tau}$, where $F(t)$ is the observed fluorescence decay, α is the amplitude, and τ is the lifetime. The lifetime and amplitude data were determined by using a nonlinear least-squares iterative reconvolution technique supplied by Edinburgh Instruments Ltd. (Imhof, 1987). [d] Standard deviation of the lifetime values. [e] Chi-squared analysis of the residuals. Chi-squared values between 1 and 1.5 are acceptable (O'Conner & Phillips, 1984c). [f] Refractive index at the sodium line. [g] Percent of energy transferred as determined by steady-state measurements. [h] Percent of energy transferred as determined by fluorescence lifetime measurements. [i] Apparent interchromophore distance as determined from steady-state measurements, assuming a unique interprobe distance. [j] Apparent interchromophore distance as determined from fluorescence lifetime measurements, assuming a unique interprobe distance. [k] Average lifetimes where $\langle\tau\rangle = \sum\alpha_i\tau_i/\sum\alpha_i$ where $i = 1$ in the absence of DNS and $i = 2$ in the presence of DNS.

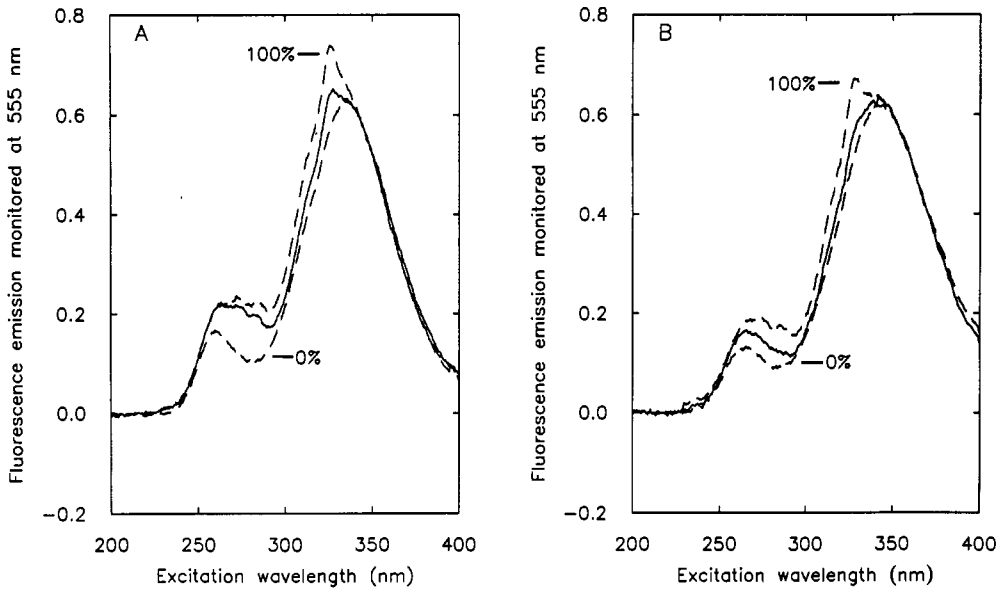

FIGURE 4: Examples of fluorescence intensity experiments, comparing effects of a denaturant, 6 M Gdn-HCl, on the efficiency of transfer at pH 8.0 and 20 °C. The transfer efficiency in the absence (A) and presence (B) of denaturant was 37% and 31%, respectively. D-Lys-N (the 100% energy transfer species, upper limit, upper dashed curve), D-OT-16 (the 0% energy transfer species, lower limit, lower dashed curve), and D-OT-16-N (—) were used to determine the efficiencies of transfer by the comparative method (see eqs 5 and 6). The excitation spectra were determined with bandwidths of 20 and 4 nm for emission and excitation, respectively.

Determination of R_0. The overlap between the corrected emission spectrum of OT-16-N and the extinction coefficient profile of D-OT-16 is extensive, as illustrated in Figure 3. The overlap integrals were determined in the absence and presence of denaturant, Tables II and III, respectively, and found to be relatively constant with a value of 5.67 (±0.07) × 10^{-15} M^{-1} cm^3. Other parameters necessary for calculating R_0 are also listed in Tables II and III. The values of the refractive index decrease with increasing temperature and increase in the presence of 6 M Gdn-HCl, as expected. Values of fluorescence lifetime and quantum yield decrease with increasing temperature because of increased collisional quenching. This was evident in both the steady-state and lifetime measurements. In addition, the presence of Gdn-HCl also results in a reduction in the values of lifetime and quantum yield and hence R_0, because Gdn-HCl is a collisional quencher.

Determination of Interprobe Distances. Energy transfer efficiencies were determined from steady-state (acceptor excitation spectra) and lifetime experiments, in the absence and presence of denaturant, and at various temperatures ranging from 1.5 to 60 °C. Examples of acceptor excitation spectra are illustrated in Figure 4; these two spectra compare the effects of 6 M Gdn-HCl on transfer efficiency at pH 8.0 and 20 °C. The efficiency of transfer in the absence and presence of denaturant, Figure 4A and 4B, was measured to be 0.37 ± 0.03 and 0.31 ± 0.02, respectively.

An example of donor lifetime measurement is illustrated in Figure 5. The decay of the donor in the absence of the acceptor, shown in Figure 5A, was fit by a monoexponential decay law with a lifetime of 10.41 ns (χ^2 = 1.27). In the presence of the acceptor, the donor lifetime exhibits multiexponential behavior with an average value of 5.60 ns (χ^2 = 1.15, when fit to two exponentials). The quality of fits to the data were also evaluated by the residuals and autocorrelation plots in each experiment. The multiexponential behavior of the donor lifetime in the presence of acceptor indicates that multiple distances, i.e., conformational states, are involved in energy transfer from the donor to the acceptor. The efficiency of transfer calculated at 20 °C from the lifetime measurements was determined to be 0.46 ± 0.03. All of the lifetime measurements and subsequent transfer efficiencies under the various conditions are listed in Tables II and III.

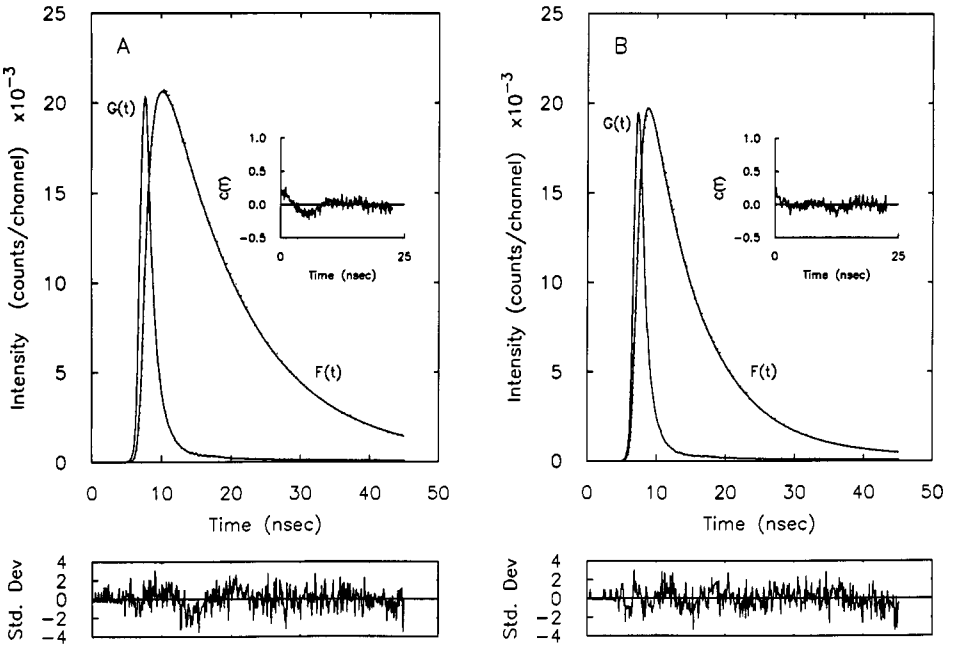

FIGURE 5: Donor fluorescence decay kinetics of OT-16-N, donor labeled species (A), and D-OT-16-N, donor-acceptor labeled species (B). The time-resolved fluorescence decays were determined by using the single photon correlation technique. The samples were excited with a nanosecond flashlamp at 316 nm. The donor decay was monitored at 345 nm with the aid of an emission monochromator. The lamp pulse profile is identified as $G(t)$, the observed fluorescence decay curve (···) is identified as $F(t)$, and the calculated decay (—) is the smooth curve drawn over the observed fluorescence (···). The residuals are plotted below the decay curves. (A) The donor decay in the absence of acceptor was monoexponential with a calculated lifetime of 10.41 ± 0.01 ns. The fit of the calculated curve was judged adequate by chi-square analysis, $\chi^2 = 1.27$. The protein concentration was 15 μM. The lower plot, below the decay profiles, illustrates the weighted residuals; these measure the deviation between the data and the fitted function with the deviation measured in units of standard deviation (Imhof, 1987). The inset shows an alternative method of assessing the goodness of fit, the autocorrelation of residuals, $C(T)$ (Grinvald & Steinberg, 1974). (B) The donor decay in the presence of acceptor exhibited a double-exponential behavior with a calculated average lifetime of 5.60 ± 0.32 ns. The fit of the calculated curve was judged adequate by chi-square analysis, $\chi^2 = 1.15$. The protein concentration was 10 μM.

The results indicate that, as the temperature is increased, the transfer efficiency increases (Tables II and III). Except for the experiments at 1.5 °C, the addition of Gdn-HCl at any other temperature decreases the transfer efficiencies (Tables II and III). Only a weak temperature dependence of the interprobe distances was observed under denaturing conditions.

It should be noted that appropriate control experiments were carried out to rule out the possibility of any intermolecular energy transfer. In these control experiments, D-OT-16 and OT-16-N were mixed together at a final peptide concentration of 20 μM, or 10 μM of each individual labeled peptide. This peptide concentration is three times that used in the experiments to determine intramolecular energy transfer. The lifetime values of the donor probe (NAA) at 20 and 60 °C were identical within experimental error to those obtained for OT-16-N in the absence of acceptor. Thus, intermolecular NET or aggregation, fostered by hydrophobic interactions, can be ruled out as contributing factor in the NET measurements.

Finally, a 10% discrepancy between the efficiencies of transfer determined by steady-state and decay measurements is observed (see Discussion).

Determination of Distance Distribution. The data were analyzed by using the procedure developed by Beechem and Haas (1989). The calculated EED distributions of the D-OT-16-N peptide under folding conditions, and the effect of temperature on those distributions, are shown in Figure 6. The most dramatic result is the change in the distribution in going from 1.5 to 20 °C. At 1.5 °C, the distribution is very broad, in contrast to the narrower distributions observed at 20, 40, and 60 °C. As the temperature increases, the average interprobe distance shifts to shorter distances. This shift in the interprobe distance is shown in Figure 7. The error symbols in Figure 7 represent the limiting values that are

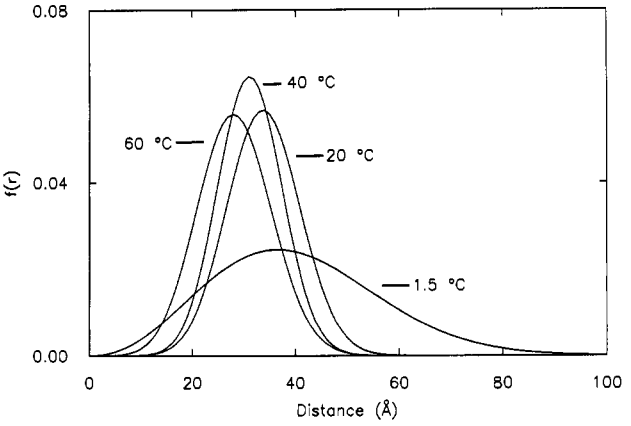

FIGURE 6: Temperature dependence of the end-to-end distance distribution functions of D-OT-16-N in the absence of denaturant as calculated from a global analysis of the donor and acceptor decay curves in the absence and presence of the acceptor as well as acceptor decay curves in the absence and presence of donor. The distance distributions were determined from data obtained at 1.5, 20, 40, and 60 °C.

characteristic of the distributions (width and average positions) as determined by rigorous error analysis (Beechem & Haas, 1989) and using a 95% confidence limit. Therefore, they are not symmetrical with respect to the best-fit values and differ for each measurement depending on the quality of the data and the noise level. A clear decreasing trend of the average EED with increasing temperature is observed.

The populations with very short or long EED (less than 10 or more than 75 Å) are less reliable. At short distances, additional mechanisms other than the Förster mechanism enhance the rate of transfer (Förster, 1948). At large distances

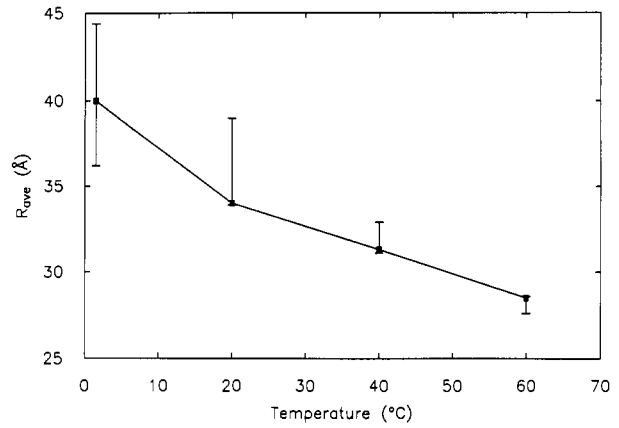

FIGURE 7: Temperature dependence of the average interprobe distance determined from the distance-distribution analysis of D-OT-16-N in the absence of denaturant (Figure 6). The error symbols were determined by a rigorous analysis procedure (Beechem & Haas, 1989). They indicate the actual range of uncertainty in each parameter caused both by the experimental noise and by the correlation with the other parameters.

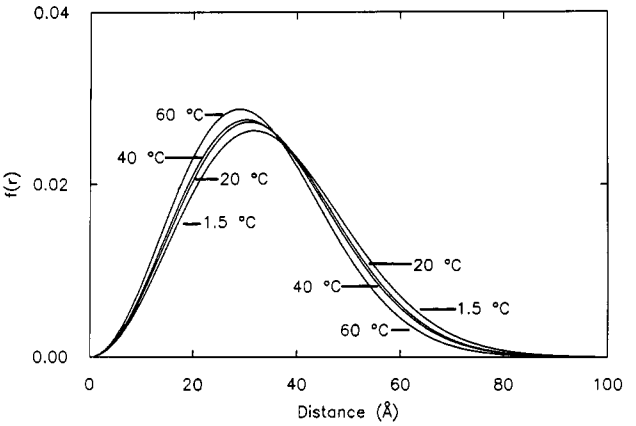

FIGURE 8: Temperature dependence of distance-distribution functions of D-OT-16-N in the presence of denaturant as calculated from a global analysis of the donor decay curves in the absence and presence of the acceptor as well as acceptor decay curves in the absence and presence of donor. The distance distributions were determined from data obtained at 1.5, 20, 40, and 60 °C.

($r > 2.5R_0$), only very low transfer probabilities are expected. Since only insignificantly small populations were found outside of the 10–75-Å range, the significance of our conclusions is not affected by these considerations. If it had been necessary, a more accurate determination of the populations at the extremes of the EED distributions would have been possible using other pairs of probes with larger and smaller R_0.

The effects of temperature on the calculated EED distributions of the D-OT-16-N peptide in the presence of 6 M Gdn-HCl are shown in Figure 8. The distributions at all temperatures are similar and are very broad because of denaturation by Gdn-HCl. It should be noted that the broad distribution in the presence of denaturant is similar to the distribution computed at 1.5 °C in the absence of denaturant. The averages of the EED distributions in the peptide under denaturing conditions differ from those obtained under folding conditions, at temperatures >1.5 °C. At these temperatures, the EED distribution is broader, with a width much like that obtained for the peptide under folding conditions at 1.5 °C. In the presence of Gdn-HCl, there is no appreciable temperature effect on the widths of the EED distributions, while the average position of the distribution decreased at higher temperatures. A more detailed tabulation of these distance distributions in the absence and presence of denaturant is given in Table IV.

Table IV: Distance Distribution Analysis Results

temp (°C)	presence of Gdn-HCl[a]	r_{ave}[b] (Å)	σ[c] (Å)	diffusion coeff (Å²/ns)
1.5	–	40.0	15.8	11
		(36.2–44.4)[d]	(10–18)	(2–25)
20.0	–	34.0	7.1	4
		(33.9–39.0)	(6.7–13.0)	(0–25)
40.0	–	31.3	6.2	1
		(31.1–32.9)	(5.0–10.9)	(0–10)
60.0	–	28.5	7.3	0.3
		(27.6–28.6)	(6.7–11)	(0–5)
1.5	+	34.5	14.4	3
		(32.4–39.6)	(10.2–16.4)	(0–12)
20.0	+	37.3	14.4	15
		(31.5–40.9)	(5.8–16.6)	(0–25)
40.0	+	31.2	13.3	10
		(29.6–36.0)	(9.7–15)	(4–25)
60.0	+	29.4	13.0	21
		(29.1–32.6)	(12.2–13.7)	(0–25)

[a] 50 mM bicine and 1 mM EDTA, pH 8.0, with (+) or without (–) 6 M Gdn-HCl. [b] Average interprobe distance calculated from a second-moment analysis (Beechem & Haas, 1989). [c] Standard deviation of the distribution [full width at half-maximum $\approx 2.354\sigma$ (Bevington, 1969a)]. [d] Values in parentheses represent the limiting values that are statistically acceptable at the 95% confidence limit.

The intramolecular segmental diffusion coefficient was calculated by the procedure of Beechem and Haas (1989). The correlation between the dependence of the fluorescence decay rates on the width and average position of the EED distributions, and its dependence on the magnitude of the intramolecular diffusion coefficient, reduce the statistical significance of the calculated parameters. The ranges of statistically acceptable values of the conformational parameters were determined by a rigorous analysis procedure (Beechem & Haas, 1989). As expected, the main uncertainty in the calculated parameters is associated with the magnitude of the intramolecular diffusion coefficients. Therefore, the range of values for the diffusion coefficients that can be accepted by the statistical analysis is relatively wide. Yet, the general trend of the effect of temperature or solvent composition on the diffusion coefficient can be detected.

The parameters characterizing the EED distributions in D-OT-16-N as a function of temperature are presented in Table IV. The formation of structure at elevated temperatures in the absence of a denaturant (folding conditions) can be seen. The values given are those of the best fit. The limiting values that are statistically acceptable at the 95% confidence level, by using an F-test (Bevington, 1969b), are given for each calculated parameter. The range of acceptable values reflects several experimental sources of noise and the correlation between the parameters. The sources of noise include the statistical quality of the data (random noise, number of counts at peak), errors in the constants used in the analysis (such as the extent of direct excitation of the acceptor), and the color sensitivity of the photomultiplier transit time. This last effect is commonly accounted for by a color shift parameter used in the analysis (Kolber & Barkley, 1986). In this study, the broad distribution of decay rates, i.e., distance distributions, coupled with the error introduced by the color shift results in the loss of some diffusion and distribution information. Despite these difficulties, the results indicate a relationship not normally expected for an unstructured peptide, i.e., the diffusion coefficient *decreases* with increasing temperature, under folding conditions. In the presence of 6 M Gdn-HCl, the diffusion coefficient *increased* with increasing temperature, as would be expected for an unstructured peptide (Table IV).

Discussion

Conformational Folding of the C-Terminal Peptide of RNase A, OT-16-DABA. The EED distributions obtained from the analysis of the measurements made under folding conditions are relatively narrow at temperatures ≥20 °C. This shows that, at room temperature and above, in the absence of a denaturant, D-OT-16-N is at least partially structured. A relatively narrow population of conformers exists at these temperatures with an average EED ranging from 28 to 34 Å (Table IV, Figure 7). With the present experimental setup, the large range of statistically acceptable values of the diffusion coefficients calls for caution in interpretation of the results. Yet, the general trend is clear: increased temperature causes a reduction of the mutual diffusion between the chain ends. These observations indicate that the ensemble of structured conformations in the distribution is stabilized by increasing temperature and, therefore, involves hydrophobic interactions (Némethy & Scheraga, 1962). Presumably, the hydrophobic interactions, strengthened with increasing temperature, give rise to the reduced conformational flexibility and dynamics of the peptide, as revealed by the shorter average EED distributions, the smaller width of the distributions, and the decreasing diffusion coefficients (Table IV). Thus, there appear to be sufficiently strong short-range hydrophobic interactions in D-OT-16-N to direct the partial folding of the peptide, as would be expected in a CFIS.

The identification of hydrophobic interactions as the stabilizing factor in D-OT-16-N is also supported by the apparent cold denaturation that occurs at 1.5 °C in the absence of 6 M Gdn-HCl. The broad distribution exhibited at this temperature is similar to the distributions generated at all temperatures in the presence of 6 M Gdn-HCl, a strong denaturant, which also appears to disrupt the hydrophobic interactions that stabilize the partially folded peptide. The implication of stabilizing intramolecular hydrophobic interactions is also supported by the apparent increasing diffusion coefficient observed with increasing temperatures in the presence of denaturant. This latter trend supports the conclusion that the peptide is unstructured in 6 M Gdn-HCl and has a considerable degree of structure in the absence of denaturant under folding conditions in which the temperature is ≥20 °C.

The correlation between the equilibrium EED distributions (width and average positions) and diffusion coefficient parameters reduces our ability to determine all parameters with a very low uncertainty. In particular, the calculated diffusion coefficients have very large ranges of statistical uncertainty. Yet, the information about the dynamic contribution to the transfer rates is not lost. It is accounted for by the width parameters of the distributions, determined by detailed rigorous error analysis (Beechem & Haas, 1989). In an attempt to minimize the error range observed in our analysis, an upper limit was placed on the diffusion coefficient in which all values of $D \geq 25$ Å^2 ns^{-1} were ignored. This limit was selected based upon previous measurements of the diffusion coefficient for a flexible peptide (Haas, et al., 1978b).

The distance distribution analysis, including diffusion, clearly indicates the existence of structure in the peptide in the absence of denaturant and at temperatures ≥20 °C, presumably arising from hydrophobic interactions due to the preponderance of nonpolar amino acids in the OT-16 peptide. These results support the theoretical CFIS model proposed by Matheson and Scheraga (1978). Yet, it should be noted that the distribution of structures exhibited by the peptide in solution appears to be predominantly nonnative, since the known distance between the C^{α} groups of His^{105} and Val^{124} in the crystal structure is only 6 Å (Wlodawer et al., 1982).

The absence of native structure in the peptide does not mean that OT-16 does not contain a CFIS. In the model of Matheson & Scheraga (1978), a CFIS need not acquire the native conformation in the early stages of folding in order to be able to direct further folding but can initially take on a nonnative conformation that is compact and restricts the amount of conformational space that the remainder of the protein has to sample. This model is directly applicable to the OT-16 peptide, in which the asparagine^{113}-proline^{114} peptide group is most likely in both the cis and trans conformations. Presumably, a compact structure in the CFIS of OT-16 can form in the initial stages of folding in RNase A, with the asparagine^{113}-proline^{114} peptide group in either the cis or trans conformation, as was also found by conformational energy calculations by Pincus et al. (1983). The nonnative conformation can then rearrange to a native one by a cis/trans isomerization in the *later* stages of folding.

This study also complements the previous work of Haas et al. (1987) that examined the fluorescence lifetime of the sole tyrosine (residue 115) in OT-16 and led to the conclusion that the tyrosine resided in at least two conformational ensembles. The distance distribution analysis of the energy transfer experiments in this study supports this earlier conclusion.

Calculations were carried out using ECEPP/2 parameters (Némethy et al., 1983) to ascertain an approximate interprobe distance for the unfolded conformation. The calculated extended-chain EED of D-OT-16-N is 83 Å, and that of the statistical-coil (Flory, 1969) is 36–38 Å. The calculated distance of 83 Å is similar to that at the upper end of the distance distributions shown in Figure 8 for the unfolded peptide. The calculated distance of 36–38 Å for the statistical-coil form is comparable to the average interprobe distances computed from the 1.5 °C data in the absence of denaturant and the distances determined at temperatures less than 60 °C in the presence of 6 M Gdn-HCl. The somewhat shorter average interprobe distances determined from the distance distribution analysis for the presumed partially ordered structure in D-OT-16-N (Figure 6) do not differ by much from the calculated values for the statistical coil. However, the sharpening of the distributions at temperatures ≥20 °C implies that partially ordered structures have formed.

The existence of primarily nonnative ordered structure could be attributed to three factors. First, it is likely that the packing of the hydrophobic side chains of OT-16-DABA differs from that observed in RNase A. In addition to the numerous close contacts in the OT-16 region in the contact map of RNase S, described by Némethy and Scheraga (1979), there are also numerous close contacts between a region extending from Ser^{50} to Ser^{80} and the OT-16 region. Thus, it seems likely that, in the absence of this Ser^{50} to Ser^{80} region in the isolated OT-16 fragment, the hydrophobic packing of the side chains in the OT-16-DABA fragment would be different from that observed in RNase A. Secondly, it is possible that native interactions are disrupted by the presence of the charged sulfonated cysteine. Sulfonation increased the solubility of this nonpolar peptide in water and also facilitated the purification of the peptide and its derivatives. A methyl disulfide derivative of OT-16-DABA was also prepared but the doubly labeled species was not soluble. The sulfonated cysteine may introduce nonnative electrostatic interactions that alter the folding pathway of the peptide. Yet, it should be pointed out that hydrophobic interactions appear to be the primary factor in the formation of a compact structure in the peptide and that the modified OT-16 is a useful model for the C-terminal CFIS.

Experiments are planned to determine the role that electrostatic interactions play in the folding of this peptide. Finally, the presence of the two fluorescent probes probably does not bias the calculated EED distributions. This conclusion is supported by several observations: (1) In another experiment (Amir & Haas, 1988), similar probes were attached to the end of a flexible peptide and no bias was observed. (2) Probe–probe interactions would be expected to increase the population of the very short distances in the EED distribution, which was not observed. (3) In the absence of ordered conformations, probe–probe interactions would be reduced by Gdn-HCl. Yet, at least in the low-temperature experiments, there seems to be no contribution to the EED distribution that is eliminated by the high Gdn-HCl concentrations.

The steady-state measurements do not contain additional information beyond that available from the fluorescence decay measurements. However, they do add an important control for the fate of the excitation energy lost by the donor. Despite this inherent control in our experimental approach, Table II shows a discrepancy between the transfer efficiencies obtained using the two methods under the following conditions. In the absence of Gdn-HCl, the steady-state measurements yielded transfer efficiencies that were lower than those obtained by analysis of donor decay only in the lower temperature experiments (1.5 and 20 °C). In the presence of Gdn-HCl, this difference was observed only in the higher temperature experiments (40 and 60 °C).

We currently do not have a clear explanation for these differences. Yet, it should be noted that the steady-state experiment is based on analysis of acceptor fluorescence only, while the $E(\tau)$ experiment is based on donor emission only. It is possible that the donor energy could be transferred, at short distances (≤15 Å), to the acceptor by a non-Förster transfer mechanism such as electron transfer, subsequently affecting acceptor fluorescence. But, this would seem to be a very unlikely event, since the calculated EEDs suggest a very small population of conformers with distances ≤15 Å. It is pertinent to note that the global analysis used for calculation of the EED distributions accounts for *both* the donor and acceptor emission information and thus reduces the effects of possible errors reflected in the comparison of the donor decay data and the excitation spectral data. Thus, no definite explanation for the deviation between the two methods can be suggested. However, since the temperature dependence of the transfer efficiency is greater in the steady-state measurements, implying more extended conformations at the lower temperatures, this can only enhance our suggestion of the existence of a CFIS in the OT-16 region of RNase A.

Despite the complications mentioned above, the D-OT-16-N peptide exhibits a partially ordered structure, i.e., an equilibrium ensemble of structures ranging from the native-like compact to extended-chain conformers, that is stabilized by hydrophobic interactions. This study demonstrates that local folding can occur in a region identified as a CFIS. Further experiments, currently in progress, are designed to improve the quality of the data and include additional type of measurements designed to improve the global analysis. These extensions of this work should enable us to reduce the uncertainities and better resolve the conformational dynamics of the partially folded protein fragments on the nanosecond time scale.

Conclusion

We have stoichiometrially labeled OT-16-DABA at the N- and C-terminal regions with probes that enabled us to monitor conformational changes by NET. The distance distribution analysis allowed us to study the conformational changes that occur on the nanosecond time scale and monitor a structural equilibrium that is present in this peptide. Sufficient evidence now exists, both experimental and theoretical, to identify OT-16 as a CFIS whose short-range hydrophobic interactions, in the absence of medium- and long-range interactions with the remainder of the RNase A molecule, can induce the formation of an ensemble of partially ordered, compact structures in the absence of denaturant.

Acknowledgments

We thank V. G. Davenport for technical assistance, T. W. Thannhauser and R. W. Sherwood of the Biotechnology Analytical and Synthesis Facility at Cornell University for the amino acid analyses, amino acid sequencing, and accessibility to the MilliGen peptide synthesizer, J. Conboy and J. Henion of the Equine Drug Testing Facility at Cornell University for the electrospray mass-spectrometry analyses, K.-H. Altmann for helpful discussions about the synthesis of the α-FMOC-γ-t-BOC-diaminobutyric acid, B. Cherayil, A. Nayeem, and R. L. Williams for the calculations of the dimensions of the extended chain and statistical coil, D. M. Rothwarf and E. E. DiBella for helpful discussions, and G. Haran and Y. Vilner of the Department of Life Sciences of Bar Ilan University for help in the analysis of the fluorescence decay curves.

References

Altmann, K.-H., & Scheraga, H. A. (1990) *J. Am. Chem. Soc. 112*, 4926–4931.
Amir, D., & Haas, E. (1988) *Biochemistry 27*, 8889–8893.
Anderson, S. R. (1969) *Biochemistry 8*, 1394–1396.
Beechem, J. M., & Haas, E. (1989) *Biophys. J. 55*, 1225–1236.
Bevington, P. R. (1969a) in *Data Reduction and Error Analysis for the Physical Sciences*, p 45, McGraw Hill, New York.
Bevington, P. R. (1969b) in *Data Reduction and Error Analysis for the Physical Sciences*, pp 195–198, McGraw Hill, New York.
Bierzynski, A., Kim, P. S., & Baldwin, R. L. (1982) *Proc. Natl. Acad. Sci. U.S.A. 79*, 2470–2474.
Chen, R. F., Edelhoch, H., & Steiner, R. F. (1969) in *Physical Principles and Techniques of Protein Chemistry* (Leach, S. J., Ed.) Part A, pp 204–208, Academic, New York.
Covey, T. R., Bonner, R. F., Shushan, B. I., & Henion, J. (1988) *Rapid Commun. Mass. Spectrom. 2*, 249–256.
de Boor, C. (1978) in *A Practical Guide to Splines*, Springer-Verlag, New York.
Edwards, S. F. (1965) *Proc. Phys. Soc., London 85*, 613–624.
Fairclough, R. H, & Cantor, C. R. (1978) *Methods Enzymol. 48*, 347–379.
Flory, P. J. (1969) in *Statistical Mechanics of Chain Molecules*, pp 8–9, Wiley-Interscience, New York.
Förster, T. (1948) *Ann. Phys. (Leipzig) 2*, 55–75.
Grinvald, A., & Steinberg, I. Z. (1974) *Anal. Biochem. 59*, 583–598.
Haas, E. (1986) in *Photophysical and Photochemical Tools in Polymer Science* (Winnik, M. A., Ed.) pp 325–350, D. Reidel Publishing Co.
Haas, E., Katchalski-Katzir, E., & Steinberg, I. Z. (1978a) *Biochemistry 17*, 5064–5070.
Haas, E., Katchalski-Katzir, E., & Steinberg, I. Z. (1978b) *Biopolymers 17*, 11–31.
Haas, E., Montelione, G. T., McWherter, C. A., & Scheraga, H. A. (1987) *Biochemistry 26*, 1672–1683.

Heinrikson, R. L., & Meredith, S. C. (1984) *Anal. Biochem. 136*, 65–74.

Hunkapiller, M. W., Granlund-Moyer, K., & Whiteley, N. W. (1986) in *Methods of Protein Microcharacterization. A Practical Handbook* (Shively, J. E., Ed.) Chapter 8, pp 223–247, Humana Press, Clifton, New Jersey.

Imhof, R. E. (1987) in *Fundamentals of Decay Curve Analysis*, Issue 2, pp 12–17, Edinburgh Instruments Ltd., Edinburgh, Scotland.

Kim, P. S., Bierzynski, A., & Baldwin, R. L. (1982) *J. Mol. Biol. 162*, 187–199.

Kolber, Z. S., & Barkley, M. D. (1986) *Anal. Biochem. 152*, 6–21.

Lakowicz, J. R. (1983) in *Principles of Fluorescence Spectroscopy*, Chapter 10, pp 303–339, Plenum Press, New York.

Matheson, R. R., Jr., & Scheraga, H. A. (1978) *Macromolecules 11*, 819–829.

McWherter, C. A., Haas, E., Leed, A. R., & Scheraga, H. A. (1986) *Biochemistry 25*, 1951–1963.

Milburn, P. J., & Scheraga, H. A. (1988) *J. Protein Chem. 7*, 377–398.

MilliGen technical note 3.10 (1987) in *Operation Manual*, MilliGen, Division of Millipore, Bedford, MA.

MilliGen technical note 4.30 (1987) in *Operation Manual*, MilliGen, Division of Millipore, Bedford, MA.

MilliGen technical note 5.21 (1987) in *Operation Manual*, MilliGen, Division of Millipore, Bedford, MA.

Mitchinson, C., & Baldwin, R. L. (1986) *Proteins 1*, 23–33.

Montelione, G. T., Arnold, E., Meinwald, Y. C., Stimson, E. R., Denton, J. B., Huang, S.-G., Clardy, J., & Scheraga, H. A. (1984) *J. Am. Chem. Soc. 106*, 7946–7958.

Montelione, G. T., & Scheraga, H. A. (1989) *Acc. Chem. Res. 22*, 70–76.

Moroder, L., Hallett, A., Wünsch, E., Keller, O., & Wersen, G. (1976) *Hoppe-Seyler's Z. Physiol. Chem. 357*, 1651–1653.

Némethy, G., & Scheraga, H. A. (1962) *J. Phys. Chem. 66*, 1773–1789.

Némethy, G., & Scheraga, H. A. (1979) *Proc. Natl. Acad. Sci. U.S.A. 76*, 6050–6054.

Némethy, G., Pottle, M. S., & Scheraga, H. A. (1983) *J. Phys. Chem. 87*, 1883–1887.

Nozaki, Y. (1972) *Methods Enzymol. 26*, 43–50.

O'Conner, D. V., & Phillips, D. (1984a) in *Time-Correlated Single Photon Counting*, Chapter 2, p 39, Academic Press, New York.

O'Conner, D. V., & Phillips, D. (1984b) in *Time-Correlated Single Photon Counting*, Chapter 6, pp 177–189, Academic Press, New York.

O'Conner, D. V., & Phillips, D. (1984c) in *Time-Correlated Single Photon Counting*, Chapter 6, pp 181–182, Academic Press, New York.

Pincus, M. R., Gerewitz, F., Wako, H., & Scheraga, H. A. (1983) *J. Protein Chem. 2*, 131–146.

Rico, M., Santoro, J., Bermejo, F. J., Herranz, J., Nieto, J. L., Gallego, E., & Jiménez, M. A. (1986) *Biopolymers 25*, 1031–1053.

Rico, M., Bermejo, F. J., Santoro, J., Nieto, J. L., Gallego, E., Herranz, J., Voskuyl-Holtkamp, I., & Schattenkerk, C. (1987) *Int. J. Pept. Protein Res. 29*, 193–206.

Sigler, G. F., Fuller, W. D., Chaturvedi, N. C., Goodman, M., & Verlander, M. (1983) *Biopolymers 22*, 2157–2162.

Silverman, D. N., Kotelchuck, D., Taylor, G. T., & Scheraga, H. A. (1972) *Arch. Biochem. Biophys. 150*, 757–766.

Still, W. C., Kahn, M., & Mitra, A. (1978) *J. Org. Chem. 43*, 2923–2925.

Stimson, E. R., Montelione, G. T., Meinwald, Y. C., Rudolph, R. K. E., & Scheraga, H. A. (1982) *Biochemistry 21*, 5252–5262.

Thannhauser, T. W., McWherter, C. A., & Scheraga, H. A. (1985) *Anal. Biochem. 149*, 322–330.

Wetlaufer, D. B. (1973) *Proc. Natl. Acad. Sci. U.S.A. 70*, 697–701.

Wlodawer, A., Bott, R., & Sjölin, L. (1982) *J. Biol. Chem. 257*, 1325–1332.

Wright, P. E., Dyson, H. J., & Lerner, R. A. (1988) *Biochemistry 27*, 7167–7175.